Kinetic Behavior of Metal Hydride Electrode by Means of AC Impedance

Chunsheng Wang*

Department of Materials Science and Engineering, Zhejiang University, Hangzhou 310027, China

ABSTRACT

A mathematical model for the electrochemical impedance spectroscopy of a metal-hydride electrode was developed. The model was used to study the effect of various parameters on predicted kinetic behavior. The simulations obtained using the model show that the first arc appearing in the higher frequency range is due to a charge-transfer reaction, the second arc in the middle frequency range represents the hydrogen transfer between the absorption and adsorption, and the third arc (or curve) at low frequency corresponds to the diffusion of absorbed hydrogen in the alloy. As the rate constant of the charge-transfer reaction, the rate constant of hydrogen transfer, and the diffusion coefficient increase, all of the three arcs moved toward higher frequency range and the diameter of the arcs decreases. The model simulations also show that the state of discharge plays an important role in the Nyquist plot of the metal-hydride electrode. The kinetic parameters used in the model predictions are those for $TiMn_{1.5}H_x$.

Introduction

Recently, nickel/metal hydride (Ni/MH) batteries have been developed and commercialized because of their high energy density, high dischargeability, long charge-discharge cycle life, and environmental cleanliness.[1] The electrode reactions at the negative and positive electrode in Ni/MH_x batteries can be expressed by

$$M + H_2O + e^- \rightleftarrows MH + OH^- \quad [1]$$

$$Ni(OH)_2 + OH^- \rightleftarrows NiOOH + H_2O + e^- \quad [2]$$

In charge/discharge processes, the concentration of H_2O and OH^- is constant.

Extensive work has been carried out on the cathodic hydrogen evolution reaction on hydrogen-absorbing metals.[2-8] By considering that the electrochemical sorption/desorption of hydrogen by and from metallic hosts is diffusion limited, Conway and Wojtowicz[5] performed numerical calculations for the time scales of the hydrogen desorption. Apart from the electrochemical and diffusion step, Yang et al.[7] also considered hydrogen transfer through the interface and established a general relationship between the overpotential and the rate of hydrogen diffusion in the electrodes, as well as the kinetic parameters characterizing the transfer of hydrogen from the absorbed to the adsorbed state. Lei et al.[8] first presented a mathematical model for the hydride electrode, i.e., the dependence of discharge capacity on discharge current and cycle life by considering the phase transformation and oxide film growth on the surface of metal particles during hydriding/dehydriding processes.

Electrochemical impedance spectroscopy (EIS) is an effective technique for analyzing the mechanisms of hydriding/dehydriding reaction for a hydride electrode.[9] Lim and Pyun[10] derived a faradaic admittance of the hydrogen absorption reaction (HAR) on a Pd membrane electrode and analyzed the diffusion-controlled HAR for fast rate hydrogen transfer and the interface-controlled HAR for slow rate hydrogen transfer from bulk to Pd surface. Kuriyama et al.[11,12] used the ac impedance method to investigate the degradation mechanism of metal hydride electrodes and activity of alloys. Using the electrochemical impedance spectroscopy (EIS) technique, Zhang et al.[9] analyzed the mechanism of the hydriding/dehydriding reaction on the hydride electrode, and proposed an equivalent circuit for the MH_x electrode. However, in Zhang's equations, the diffusion of hydrogen and the phase transformation was not considered, which was a very important factor in the electrochemical hydriding/dehydriding reaction for the hydride electrode. Thus to date, the electrode kinetics of the hydriding/dehydriding reaction have not been well elucidated.

In this present paper, ac impedance involving HAR for hydride electrodes with different spherical geometry is theoretically derived by considering the phase transformation in hydriding/dehydriding processes. The factors affecting kinetics of the reaction have been analyzed. Some equations deduced by Zhang et al.[9] are also included here for completeness.

AC Impedance Modeling

Basic assumptions and model development.—The electrochemical charge-discharge test and ac impedance measurement were carried out in a sealed standard three-electrode cell, in which the counter electrode was nickel oxyhydroxide, the reference electrode was Ag/AgCl, and the electrolyte used in all experiments was 6 M KOH solution. The electrode is considered initially to be uniformly charged with hydrogen with a bulk concentration $C_{\alpha\,max}$ for solid solution phase electrode and C_β for the hydride electrode, expressed in mole hydrogen concentration stored in the host metal. Thus, the molar concentration quotient in the bulk can be expressed according to Wagner[13] as $x_\alpha = C_\alpha/N$, where N is the total molar number of interstitial sites available for hydrogen per unit volume of the host metal, and x_s denotes the molar occupation quotient of absorbed hydrogen in the near-surface.

The hydriding reaction involves a charge-transfer step followed by the surface transition from the adsorbed site on the electrode surface to the absorbed site in the near-surface

* Electrochemical Society Active Member.

region and then the diffusion of absorbed hydrogen from the near-surface into the bulk. When the concentration of the absorbed hydrogen in the bulk reaches the maximum solubility of hydrogen in the metals the phase transition (forming hydride) occurs. Suppose the pressure in the sealed cell is higher than the hydrogen pressure equilibrated with $C_{\alpha\,max}$ or C_β, so that the hydrogen evolution reaction can be neglected during ac impedance measurements

$$M + H_2O + e^- \underset{k_{-1}}{\overset{k_1}{\rightleftarrows}} MH_{ads} + OH^- \quad [3]$$

$$MH_{ads} \underset{k_{-2}}{\overset{k_2}{\rightleftarrows}} MH_{abs(surface)} \quad [4]$$

$$MH_{abs(surface)} \xrightarrow{J_{(diffusion)}} MH_{abs(bulk,\alpha)} \quad [5]$$

or

$$MH_{abs(bulk,\alpha)} \xrightarrow{\text{phase transition}} MH_{abs(bulk,\beta)} \quad [6]$$

In order to analyze and interpret the experimental results, it is necessary to derive a theoretical expression for the impedance for the above process.

The current density for the charge-transfer step (reaction 3) can be expressed as follows[9]

$$i = \vec{i} - \overleftarrow{i} = nF\left[k_1 a_{H_2O} C^o_{H_2O}(1-\theta)\exp\left(-\frac{\alpha nF}{RT}\varphi\right) - k_{-1} a_{OH^-} C^o_{OH^-}\theta \exp\left(\frac{\beta nF}{RT}\varphi\right)\right]$$

$C^o_{H_2O}$ and $C^o_{OH^-}$ are the concentration of H_2O and OH^- in the reference state (here 1 M). Therefore $C^o_{H_2O} = C^o_{OH^-} = 1$. The above equation can be rewritten as

$$i = \vec{i} - \overleftarrow{i} = nF\left[k_1 a_{H_2O}(1-\theta)\exp\left(-\frac{\alpha nF}{RT}\varphi\right) - k_{-1} a_{OH^-}\theta \exp\left(\frac{\beta nF}{RT}\varphi\right)\right] \quad [7]$$

In ac impedance studies the variables are composed of a steady-state component plus an alternating component

$$i = \bar{i} + \tilde{i}, \quad \theta = \bar{\theta} + \tilde{\theta}, \quad \varphi = \bar{\varphi} + \tilde{\varphi} \quad [8]$$

differentiation of Eq. 7 gives

$$\frac{d\tilde{i}}{dt} = nF\left\{-\left[\frac{\vec{i}}{(1-\theta)nF} + \frac{\overleftarrow{i}}{\theta nF}\right]\frac{d\tilde{\theta}}{dt} - \frac{1}{RT}(\alpha\vec{i} + \beta\overleftarrow{i})\frac{d\tilde{\varphi}}{dt}\right\} \quad [9]$$

where $\tilde{i}$, $\tilde{\theta}$, and $\tilde{\varphi}$ are at the same frequencies as expressed by

$$\tilde{B} = B_0 \exp(j\omega t) \quad [10]$$

where $\tilde{B}$ represents $\tilde{i}$, $\tilde{\theta}$, and $\tilde{\varphi}$ and B_0 is the amplitude of these variables. The time derivative of Eq. 10 is

$$\frac{d\tilde{B}}{dt} = j\omega\tilde{B} \quad [11]$$

Thus, Eq. 9 can be further simplified as follows

$$\tilde{i} = -\left[\frac{\vec{i}}{(1-\theta)} + \frac{\overleftarrow{i}}{\theta}\right]\tilde{\theta} - \frac{nF}{RT}(\alpha\vec{i} + \beta\overleftarrow{i})\tilde{\varphi} \quad [12]$$

The interfacial impedance of MH_x electrode Z is

$$Z = -\frac{\tilde{\varphi}}{\tilde{i}} \quad [13]$$

From Eq. 12 and 13 we obtain

$$Z = Z_f + Z_h \quad [14]$$

where

$$Z_f = \frac{RT}{nF(\alpha\vec{i} + \beta\overleftarrow{i})} = R_{ct} \quad [15]$$

and

$$Z_h = \frac{RT}{nF(\alpha\vec{i} + \beta\overleftarrow{i})}\left(\frac{\vec{i}}{1-\theta} + \frac{\overleftarrow{i}}{\theta}\right)\frac{\tilde{\theta}}{\tilde{i}} \quad [16]$$

$Z_f (= R_{ct})$ is the impedance due to the charge-transfer reaction, and Z_h is the impedance due to the hydrogen transfer between absorbed and desorbed state and hydrogen diffusion in the bulk of the electrodes which occur in series. Therefore, the contribution to the impedance is due to the three steps: charge-transfer reaction, hydrogen transfer between the absorbed to the adsorbed state, and hydrogen diffusion in the bulk of the electrode, which occur in series.

In small-signal ac conditions, the R_{ct} (charge-transfer resistance) and $RT/nF(\alpha\vec{i} + \beta\overleftarrow{i})$ $(\vec{i}/1-\theta + \overleftarrow{i}/\theta)$ can be considered as constants.

Consider Eq. 7 being at equilibrium, and neglect the variation of a_{OH^-} and a_{H_2O} in small-signal ac conditions, then

$$\vec{i} = \overleftarrow{i} = i_o = nFk_1 a_{H_2O}(1-\bar{\theta})\exp\left(-\frac{\alpha nF}{RT}\varphi\right) = nFk_{-1} a_{OH^-}\bar{\theta}\exp\left(\frac{\beta nF}{RT}\varphi\right) \quad [17]$$

Let

$$\alpha \approx 0.5, \quad \beta \approx 0.5, \quad \bar{\theta} >> \tilde{\theta} \quad [18]$$

$$A = \frac{a_{OH^-}}{a_{H_2O}}\exp\left(\frac{nF}{RT}\varphi\right) \quad [19]$$

$$K_1 = \frac{k_{-1}}{k_1} \quad [20]$$

$$K_2 = \frac{k_{-2}}{k_2} \quad [21]$$

Combining Eq. 15-21, Z_f and Z_h can be obtained as follows

$$Z_f = R_{ct} = \frac{RT}{nF(\alpha\vec{i} + \beta\overleftarrow{i})} \approx \frac{RT}{nFi_o} = \frac{RT}{n^2F^2k_{-1}a_{OH^-}\exp\left(\frac{\beta nF}{RT}\varphi\right)}(K_1A + 1) \quad [22]$$

$$Z_h = \frac{RT}{nF(\alpha\vec{i} + \beta\overleftarrow{i})}\left(\frac{\vec{i}}{1-\theta} + \frac{\overleftarrow{i}}{\theta}\right)\frac{\tilde{\theta}}{\tilde{i}} \approx \frac{RT}{nF\bar{\theta}(1-\bar{\theta})}\frac{\tilde{\theta}}{\tilde{i}} = \frac{RT}{nF}\left[\sqrt{K_1A} + \frac{1}{\sqrt{K_1A}}\right]^2\frac{\tilde{\theta}}{\tilde{i}} \quad [23]$$

In order to obtain $\tilde{\theta}/\tilde{i}$, reaction 4 is taken into account. By assuming first-order kinetics for the absorption reaction, the surface transition reaction can be expressed as follows[7]

$$i - k_2nF\theta(1-x_s) + k_{-2}nFx_s(1-\theta) = nF\Gamma\frac{d\theta}{dt} \quad [24]$$

where Γ denotes the maximum amount of hydrogen that can be adsorbed on the surface, θ is the hydrogen coverage at the surface, β the symmetry coefficient, φ the potential, F the Faraday constant, R the gas constant, T the temperature in kelvin, and a_{OH^-} and a_{H_2O} are the activities of OH^- and H_2O in solution, respectively.

In Ni/MH battery, the concentration of OH^- and H_2O is constant (see reaction 1 and 2), and the activity change of OH^- and H_2O in solution can be neglected because of the high diffusion rate of OH^- and H_2O and the higher poros-

ity of the metal-hydride electrode.[14] Thus, the current density becomes only a function of the degree of coverage of adsorbed hydrogen on the surface θ and the electrode potential φ.

By introducing the alternating component, Eq. 24 can be modified as

$$\bar{i} + \tilde{i} - k_2 nF(\bar{\theta} + \tilde{\theta})(1 - \bar{x}_s - \tilde{x}_s) + k_{-2} nF(\bar{x}_s + \tilde{x}_s)(1 - \bar{\theta} - \tilde{\theta}) = nF\Gamma \frac{d(\theta + \tilde{\theta})}{dt} \quad [25]$$

At the equilibrium potential

$$\bar{i} = 0, \quad -k_2 nF\bar{\theta}(1 - \bar{x}_s) + k_{-2} nF\bar{x}_s(1 - \bar{\theta}) = 0 \quad [26]$$

Because of small amplitude of $\tilde{x}_s$ and $\tilde{\theta}$ in small-signal ac conditions, the value of $(k_{-2} - k_2)\tilde{x}_s\tilde{\theta}$ is much smaller than that of $\tilde{x}_s$ and $\tilde{\theta}$, and can be neglected.

From Eq. 26, the dependence of $\bar{x}_s$ on the surface coverage $\bar{\theta}$ is obtained as

$$\bar{x}_s = \frac{k_2\bar{\theta}}{k_2\bar{\theta} + k_{-2}(1 - \bar{\theta})} \quad [27]$$

By substitution of Eq. 27 into Eq. 25 and neglecting $(k_{-2} - k_2)\tilde{x}_s\tilde{\theta}$

$$\frac{\tilde{i}}{nF} - \frac{k_{-2}k_2\tilde{\theta}}{k_2\bar{\theta} + k_{-2}(1 - \bar{\theta})} + [k_2\bar{\theta} + k_{-2}(1 - \bar{\theta})]\tilde{x}_s = \Gamma j\omega\tilde{\theta} \quad [28]$$

For hydrogen storage hosts with any geometry (plates, cylinders, or spheres), the hydrogen diffusion flux J is proportional to the surface hydrogen concentration (see next section). The alternating component of flux $\tilde{J}$ at electrode surface can be expressed as

$$\tilde{J}_i = \tilde{C}_s f(j\omega, D)_i = N\tilde{x}_s f(j\omega, D)_i \quad [29]$$

where i = p, c, s, sp for planar, cylindrical, spherical electrodes, and spherical electrode with phase transformation, respectively.

According to the mass balances at the electrode surface

$$\tilde{i} - nF\Gamma j\omega\tilde{\theta} = nF\tilde{J}_i \quad [30]$$

Combining Eq. 28, 29, and 30

$$\frac{\tilde{i}}{\tilde{\theta}} = \frac{nFk_2k_{-2}}{(k_2\bar{\theta} + k_{-2}(1 - \bar{\theta})\left[1 + \frac{k_2\bar{\theta} + k_{-2}(1 - \bar{\theta})}{Nf(j\omega, D)_i}\right]} + \Gamma j\omega \quad [31]$$

and combining Eq. 14, 22, 23, and 31

$$Z = \frac{RT}{n^2F^2k_{-1}a_{OH^-}\exp\left(\frac{\beta nF}{RT}\varphi\right)}(K_1A + 1) + \left\{\frac{F^2\Gamma}{RT}\left(\sqrt{K_1A} + \frac{1}{\sqrt{K_1A}}\right)^{-2} j\omega + \left[\frac{RT}{n^2F^2k_{-2}}\left(1 + \frac{1}{K_1A}\right)(1 + K_1K_2A) + \left(\sqrt{K_1K_2A} + \sqrt{\frac{1}{K_1K_2A}}\right)^2 \frac{RT}{n^2NF^2f(j\omega, D)_i}\right]^{-1}\right\}^{-1} = R_{ct} + \left\{C_{ad}j\omega + \left[R_{ab} + \frac{\sigma}{f(j\omega, D)_i}\right]^{-1}\right\}^{-1} \quad [32]$$

where

$$C_{ad} = \frac{F^2\Gamma}{RT}\left(\sqrt{K_1A} + \frac{1}{\sqrt{K_1A}}\right)^{-2} \quad [33]$$

$$R_{ab} = \frac{RT}{n^2F^2k_{-2}}\left(1 + \frac{1}{K_1A}\right)(1 + K_1K_2A) \quad [34]$$

$$\sigma = \left(\sqrt{K_1K_2A} + \sqrt{\frac{1}{K_1K_2A}}\right)^2 \frac{RT}{n^2NF^2} \quad [35]$$

R_{ct} and A are defined in Eq. 22 and 19, respectively.

Considering the resistance of the solution R_s and a double-layer capacitance C_{dl}, the total impedance of the metal-hydride electrode is

$$Z_t = R_s + \cfrac{1}{j\omega C_{dl} + \cfrac{1}{R_{ct} + \cfrac{1}{j\omega C_{ad} + \cfrac{1}{R_{ab} + \cfrac{\sigma}{f(j\omega, D)_i}}}}} \quad [36]$$

The equivalent circuit corresponding to Eq. 36 is shown in Fig. 1. Equation 36 is the total impedance of the metal-hydride electrode with neglecting the hydrogen evolution. Thus is is only suitable to HAR of metal-hydride electrode. Equation 36 and the equivalent circuit are similar to the reports of Lim and Pyun[15] in appearance. However, the parameters of equation are quite different. From Eq. 33 and 34, it can be found that the C_{ad} increases with the maximum coverage degree of absorbed hydrogen. Therefore C_{ad} is the adsorption capacitance. Also R_{ab} increases with decreasing the desorption rate constant k_{-2} and at certain potential and equilibrium constant K_2, the value of k_{-2} reflect the rate of hydrogen transfer between absorbed and desorbed state, thus R_{ab} is absorption resistance. Physical significance of the parameters C_{ad} and R_{ab} have been discussed elsewhere.[16]

$f(j\omega, D)$ of two-phase electrode with spherical symmetry.—$f(j\omega, D)_i$, (i = p, c, s) have been deduced by Jacobesen and West.[17] $f(j\omega, D)$ for a single-phase electrode with spherical symmetry is[17]

$$f(j\omega, D)_s = \frac{\sqrt{j\omega D}}{\tanh\left(r_o\sqrt{\frac{j\omega}{D}}\right)} - \frac{D}{r_o} \quad [37]$$

where r_o is the radius of metal particles, D is the diffusion coefficient of hydrogen in the metal particles.

The galvanostatic discharge process of hydride electrodes in a two-phase region can be well described by the shrinking untransformed hydride-core model.[8] It is logical to believe that the state of discharge for two-phase electrodes would not change during a small signal ac measurement (potential oscillation ≤10 mV). Therefore the size of the untransformed hydride-core r_h is unchanged during

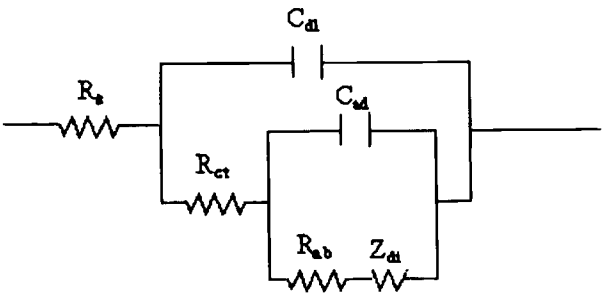

Fig. 1. Equivalent circuit for metal-hydride electrodes.

a small-signal ac measurement. For a spherical electrode, the boundary condition is

$$r = r_h, \quad \Delta C = 0$$

$$r = r_o, \quad \Delta C = C_s \exp(j\omega t)$$

The hydrogen diffusion flux is

$$\tilde{J}_{surf} = \tilde{C}_s \left[\frac{\sqrt{j\omega D}}{\tanh\left[(r_o - r_h)\sqrt{\frac{j\omega}{D}}\right]} - \frac{D}{r_o} \right]$$

From Eq. 29, $f(j\omega, D)_{sp}$ is obtained as follows

$$f(j\omega, D)_{sp} = \frac{\sqrt{j\omega D}}{\tanh\left[(r_o - r_h)\sqrt{\frac{j\omega}{D}}\right]} - \frac{D}{r_o} \quad [38]$$

Comparing Eq. 38 with Eq. 37, we concluded that the hydrogen diffusion in the $\alpha + \beta$ region is faster than in the single phase due to $0 < r_h < r_o$.

The relationship between r_h and the fraction of α phase X_α was obtained by Lei et al.[8]

$$\frac{r_h}{r_o} \approx (1 - X_\alpha)^{1/3}$$

where

$$X_\alpha = \frac{V_\alpha}{V_\alpha + V_\beta}$$

V_α and V_β are the volume of α and β phase in two-phase electrode, respectively. Equation 38 is rewritten as

$$f(j\omega, D)_{sp} = \frac{\sqrt{j\omega D}}{\tanh\left[r_o[1 - (1 - X_\alpha)^{1/3}]\sqrt{\frac{j\omega}{D}}\right]} - \frac{D}{r_o} \quad [39]$$

Determination of parameters.—The parameters of the $TiMn_{1.5}H_x$ electrode are used in these simulations. From the fit of the experimental data to the theoretical concentration dependence Yang et al.[18] calculated several characteristic parameters of the $TiMn_{1.5}$ electrode as follows: the maximum value of the storable hydrogen concentration $N = 0.02$ mol/cm^3, the symmetry coefficient for the electrochemical reaction $\beta \approx 0.5$, $K_2 = k_{-2}/k_2 = 2.37$, the solubility of H in the bulk at 1 atm $X_m = 0.69$, the equilibrium potential $\varphi_o = -1.06$ V vs. Ag/AgCl and the constant $a = -1.89$, and α_{H_2O}, in a 6 M KOH solution 0.68 at 25°C. [19] The $K_1 (= k_{-1}/k_1)$ and α_{OH^-} is calculated as 0.94 and 7.43×10^{17}, respectively, according to the equations $X_m = K_1K_2/1 + K_1K_2$ and $\varphi_o = -RT/F \ln(\alpha_{OH^-}/K_1K_2\alpha_{H_2O})$, which were deduced by Yang et al.[18] On the basis of the equation $a = -(1 - \beta) \ln K_2 + \ln[F(k_{-1}\alpha_{OH^-})^{(1-\beta)}(k_1\alpha_{H_2O})^{\beta}]$ the k_1 was determined as 3.50×10^{-15} cm/s. The value of k_2 was between 10^{-5} and 10^{-7} mol/cm^2 s, [20] the specific double-layer capacitance of the active alloy C_{dl} and diffusion coefficient D are in the range of the generally accepted value of 2×10^{-5} F/cm^2 [9] and $10^{-7} \sim 10^{-10}$ cm^2/s, [14] respectively. The other parameters chosen were $\Gamma = 7.5 \times 10^{-10}$ mol/cm^2, [10] $r_o = 10^{-3}$ cm for the spherical electrode, $R_s = 0.1\ \Omega$ cm^2, $RT/F = 0.0256$ V, $F = 96{,}487$ A s/mol = 96,487 J/V mol.

Substitute above parameters into Eq. 22, 33, 34, 35, 37, and 39 the characteristic parameters of Eq. 36 are obtained

$$R_{ct} = \frac{3.58 \times 10^{-25}[1.027 \times 10^{18} \exp(38.95\varphi) + 1]}{k_{-1} \exp(19.48\varphi)} \quad [40]$$

$$C_{ad} = 2.82 \times 10^{-3}\left[1.013 \times 10^{9} \exp(19.48\varphi) + \frac{1}{1.013 \times 10^{9} \exp(19.48\varphi)}\right]^{-2} \quad [41]$$

$$R_{ab} = \frac{2.661 \times 10^{-7}}{k_{-2}}\left[1 + \frac{1}{1.027 \times 10^{18} \exp(38.95\varphi)}\right](1 + 2.43 \times 10^{18} \exp(38.95\varphi) \quad [42]$$

$$\sigma = 1.33 \times 10^{-5}\left[1.56 \times 10^{9} \exp(19.48\varphi) + \frac{1}{1.56 \times 10^{9} \exp(19.48\varphi)}\right]^{2} \quad [43]$$

$$f(j\omega, D)_s = \frac{\sqrt{j\omega D}}{\tanh\left(10^{-3}\sqrt{\frac{j\omega}{D}}\right)} - \frac{D}{10^{-3}} \quad [44]$$

$$f(j\omega, D)_{sp} = \frac{\sqrt{j\omega D}}{\tanh\left[10^{-3}[1 - (1 - X_\alpha)^{1/3}]\sqrt{\frac{j\omega}{D}}\right]} - \frac{D}{10^{-3}} \quad [45]$$

$$R_s = 0.1\ \Omega\ \text{cm}^2 \quad C_{dl} = 2 \times 10^{-5}\ \text{F/cm}^2 \quad [46]$$

In all above equations φ represents the electrode potential for single-phase electrodes. If the electrode consists of a two-phases (metal-hydride), φ presents the plateau potential φ_{plat}.

In the following sections we analyze the effects of electrode potential φ (or φ_{plat}), rate constants k_{-1}, k_{-2}, diffusion coefficient of hydrogen D, state of discharge (SOD) which has a relationship with potential φ for single-phase electrode, and X_α for two-phase electrode, on EIS of the hydride electrodes.

Discussion

Mechanism of the electrode hydriding/dehydriding reaction.—The hydride electrode is a stable, linear, and causal system for impedance studies.[9] Suppose that the potential plateau of a hydride electrode φ_{plat} is at -1 V vs. Ag/AgCl, at which the phase separation appears, and that the pressure in the seal-cell to be higher than the plateau pressure of hydrogen, therefore the HER can be neglected. Based on Eq. 36, 40-43, and 45-46 the typical impedances of the two-phase electrode with spherical symmetry measured at $\varphi_{plat} = -1$ V, $X_\alpha = 0.4$, $k_{-1} = 3.29 \times 10^{-15}$ cm s^{-1}, $k_{-2} = 1.19 \times 10^{-5}$ mol cm^{-2} s^{-1}, $D = 3 \times 10^{-8}$ cm^2 s^{-1} is illustrated in the Nyquist plots (Fig. 2a). The Nyquist plot shows three arcs in the entire frequency region. The arc in the higher frequency range represents the charge-transfer step at the electrode/solution interface, the second arc corresponds to the hydrogen transfer reaction between the absorbed and adsorbed state, and the arc in the low frequency range represents the impedance for finite spherical diffusion in the two-phase electrode. As diffusion coefficient of hydrogen decreases from 3×10^{-8} to 5×10^{-10} cm^2/s, the two arcs in the higher frequency range gradually disappear and the arc in the low frequency range becomes larger, yielding an initially short linear region with a slope of about 45° as shown in Fig. 2b, which does not appear at higher diffusion coefficient (Fig. 2a). We attributed the 45° linear line to Warburg diffusion because, for a finite spherical diffusion electrode with Nernstian diffusion layer, the ac impedances behavior in the high-frequency region can be simplified as Warburg impedance.[17] Zhang et al.[9] attributed the arc in the higher frequency region to the impedance between the current collector and the active material, the semicircle in the middle frequency range to particle to particle of MH_x

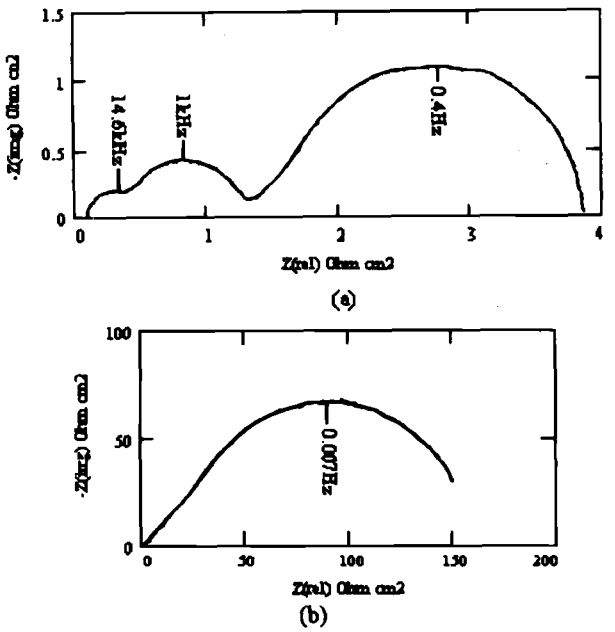

Fig. 2. Typical Nyquist plot of MH_x electrode with spherical symmetry simulated based upon Eq. 36, 40-43, and 45-46 at different values of D ($cm^2\ s^{-1}$): (a) $D = 3 \times 10^{-8}$, (b) $D = 5 \times 10^{-10}$, with the parameters of $k_{-1} = 3.289 \times 10^{-15}$ cm s^{-1}, $k_{-2} = 1.185 \times 10^{-5}$ mol $cm^{-2}\ s^{-1}$, $X_\alpha = 0.4$, $\varphi_{plat} = -1$ V vs. Ag/AgCl.

electrode, and the arc in the low frequency range to a charge-transfer step at the electrode/solution interface. Two points in Zhang et al.'s interpretation are worth discussing. First, from the EIS principle we know that the step with the small time constant would have a fast reaction rate. In an examination of their Nyquist plot, we find that the size of Ni mesh substrates and the kind of binder material do not affect the characteristic frequency $f_i^*(= 1/2\pi\tau_i)$, but only change their resistances. Therefore we believe the contact surface areas of the current collector-to-pellet and particle-to-particle do not affect the reaction rate of the two steps in the high frequency region, and the arcs in the higher frequency range do not represent the impedance of current collector-to-pellet and particle-to-particle. Second, if the hydrogen transfer rate and the hydrogen diffusion rate are relatively faster than that of the charge-transfer reaction as Zhang et al. state, the two arcs for surface transition and hydrogen diffusion may appear in an even higher frequency range than that for the charge-transfer reaction or they are overlapped by the arcs of their three steps. In the former case there may exist five arcs in the entire frequency region. Unfortunately no more than three arcs have been reported in ac impedance for Ni/MH_x so far. In the latter case, the three arcs may be attributed to the five steps. Therefore the three arcs represent the charge-transfer reaction, surface transition, and hydrogen diffusion, respectively. Also the experimental results reported by Zhang et al. can be satisfactorily explained by the present model.

Characteristics of EIS for metal-hydride electrode with flat potential plateau.—From the EIS principle we know whether the arcs of the above three separate steps depend on the difference of characteristic frequency among the three steps and their resistances. Moreover, the characteristic frequency of a step $f_i^*(= 1/2\pi\tau_i)$, is proportional to the reciprocal of the time constant τ_i. Therefore the arc of the step with the fast reaction rate appears in the high frequency range, and the arc at low frequency corresponds to the step with the slow reaction rate. The arcs of the steps with nearly the same time constant overlapped. When the differences of the time constants between the three steps are small and the differences of their resistance are large, the three arcs also overlapped.

The time constant of the charge-transfer reaction τ_e can be expressed as follows

$$\tau_e = R_{ct} \times C_{dl} = \frac{7.16 \times 10^{-30}[1.03 \times 10^{18} \exp(38.95\varphi) + 1]}{k_{-1} \exp(19.48\varphi)} \quad [47]$$

and the time constant of hydrogen transfer between the absorbed state and adsorbed state τ_a is

$$\tau_a = R_{ab} \times C_{ad} = \frac{\Gamma(1 + K_1K_2A)}{k_{-2}(1 + K_1A)}$$

$$= \frac{7.5 \times 10^{-10}[1 + 2.43 \times 10^{18} \exp(38.95\varphi)]}{k_{-2}[1 + 1.03 \times 10^{18} \exp(38.95\varphi)]} \quad [48]$$

For the finite spherical diffusion of adsorbed hydrogen in a hydride electrode with a flat potential plateau, the time constant of the arc in the low frequency region τ_d is obtained according to its equivalent circuit (see Fig. 9 and Appendix).

$$\tau_d = (R_2 + R_3)C_3 = \frac{r_o^2[1 - (1 - X_\alpha)^{1/3}]^2}{3D}\left[\frac{1}{(1 - X_a)^{1/3}} + \frac{1}{5}\right]$$

$$= \frac{10^{-6}[1 - (1 - X_\alpha)^{1/3}]^2}{3D}\left[\frac{1}{(1 - X_a)^{1/3}} + 0.2\right] \quad [49]$$

From Eq. 47 and 48 τ_e and τ_a at different plateau potential of two-phase electrodes (or potential of single-phase electrodes) are calculated with the parameters of $k_{-1} = 3.29 \times 10^{-15}$ cm s^{-1}, $k_2 = 2.37 \times 10^{-5}$ mol $cm^{-2}\ s^{-1}$ (Fig. 3). From Fig. 3, we can see that τ_e and τ_a depend on the plateau potential of the two-phase electrode (or potential of the single electrode). With decreasing plateau potential, the time constant of charge-transfer reaction τ_e decreases fast initially and then slowly. But the time constant of the hydrogen transfer reaction τ_a is almost unchanged in the potential range above -1 V, and then decreases rapidly with decreasing plateau potential, at -0.88 V τ_e and τ_a have the same value. Therefore, when the plateau potential decreases from -0.8 to -1 V, the arc of the charge-transfer reaction moves quickly toward the higher frequency range, but the arc of the hydrogen transfer reaction remains stable. At a plateau potential above -0.88 V the arc of the hydrogen transfer reaction appears at the higher frequency region than that for the arc of charge-transfer reaction. However, two separate arcs are

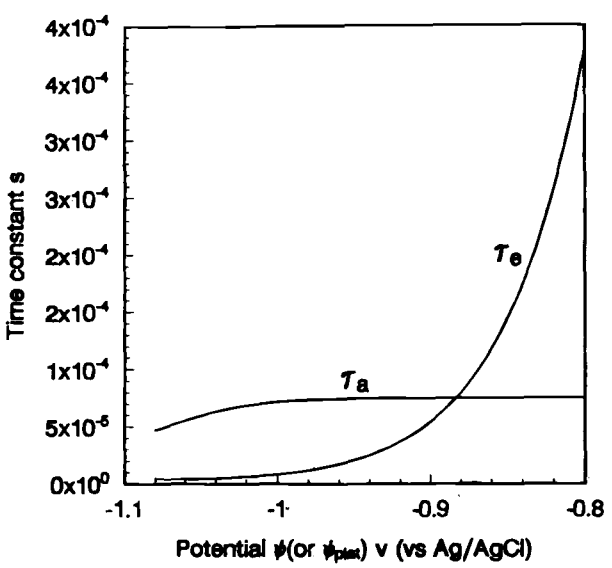

Fig. 3. Effect of plateau potential φ_{plat} (or potential φ) on τ_e and τ_a. τ_e and τ_a are simulated based on Eq. 47 and 48 with the parameters of $k_{-1} = 3.289 \times 10^{-15}$ cm s^{-1}, $k_{-2} = 2.37 \times 10^{-5}$ mol $cm^{-2}\ s^{-1}$.

not found, since at this potential range the ratio of R_{ab} to R_{ct} is very high (see Fig. 7). The arc of charge-transfer overlaps with the arc of the hydrogen transfer reaction. As to the hydrogen diffusion, the τ_d depends only on the fraction of the α phase (see Eq. 49), and it increases with fraction of the α phase as shown in Fig. 4. Therefore, with increasing of state of discharge (i.e., X_a increases), the arc of hydrogen diffusion moves toward the low frequency range. From the above analysis we conclude that the dimensionless parameters τ_e/τ_a and τ_a/τ_d can be used to assess whether or not the three arcs overlap. However the determination of those three time constants is usually difficult, only the reaction rate constant k_1 (or k_{-1}), k_2 (or k_{-2}) and hydrogen diffusion coefficient D can be easily measured by electrochemical methods.[18,21] So we expect to use the parameters k_{-1}/k_{-2} (= K_{ea}) and k_{-2}/D (= K_{ad}) to assess the relative frequency positions of the three steps. If we can obtain K_{eac} and K_{adc}, which are the values of k_{-1}/k_{-2} and k_{-2}/D at critical condition $\tau_e = \tau_a$, and $\tau_a = \tau_d$, respectively, k_{ea}/K_{eac} and K_{ad}/K_{adc} would be more convenient parameters to assess the relative frequency position of the three steps.

From Eq. 47 and 48 and $\tau_e = \tau_a$, K_{eac} can be obtained

$$K_{eac} = \left(\frac{k_{-1}}{k_{-2}}\right)_c = \frac{9.55 \times 10^{-21}[1 + 1.03 \times 10^{18} \exp(38.95\varphi)]^2}{\exp(19.48\varphi)[1 + 2.43 \times 10^{18} \exp(38.95\varphi)]} \quad [50]$$

From Eq. 48 and 49 and $\tau_a = \tau_d$

$$K_{adc} = \left(\frac{k_{-2}}{D}\right)_c = \frac{2.25 \times 10^{-3}[1 + 2.43 \times 10^{18} \exp(38.95\varphi)]}{[1 + 1.03 \times 10^{18} \exp(38.95\varphi)][1 - (1 - X_\alpha)^{1/3}]^2\left[\frac{1}{(1 - X_\alpha)^{1/3}} + 0.2\right]} \quad [51]$$

where K_{eac} is the critical rate constant ratio of the backward charge-transfer reaction to hydrogen transfer from absorbed to adsorbed state, and K_{adc} is the critical ratio of the rate constant of hydrogen transfer from absorbed to adsorbed state to the diffusion coefficient of hydrogen, respectively. If $K_{ea} > K_{eac}$ and $K_{ad} > K_{adc}$, the arcs at decreasing frequency correspond to first, the charge-transfer, then the hydrogen transfer, and finally the hydrogen diffusion. The K_{eac} vs. plateau potential is shown in Fig. 5 and K_{adc} vs. plateau potential, fraction of the α phase is shown in Fig. 6.

Because the values of K_1 (= k_{-1}/k_1) and K_2 (= k_{-2}/k_2) are constant, the K_{ea} reflects the rate constant ratio of the charge-transfer reaction to the hydrogen transfer reaction, and K_{ad} reflects the ratio of the rate constant of the hydrogen transfer reaction to the diffusion coefficient of hydrogen, respectively. From Fig. 5 and 6, we can see that with decreasing plateau potential, K_{eac} decreases first rapidly and then slowly. K_{adc} is almost unchanged in the potential range $-0.8 \sim -1$ V, and then decreases with further decreasing plateau potential. If $K_{ea} > K_{eac}$ and $K_{ad} > K_{adc}$, with decreasing potential, K_{ea}/K_{eac} and K_{ad}/K_{adc} would become larger, but R_{ct}, R_{ab}, and R_d would become smaller (see Fig. 7). Thus the arcs of the three steps would move toward the high frequency range and gradually separate. With increasing X_α, K_{adc} also decreases, but R_d increases more rapidly. Therefore at a high state of discharge the two arcs in the higher frequency range may be overlapped by the arc of the hydrogen diffusion. From the above analysis, we conclude that for a two-phase electrode the arcs of the three steps may separate at a low state of discharge and at about −1 V of potential.

Effect of the state of discharge on EIS of single-phase electrode with spherical symmetry.—For the single-phase electrode (X_α = 1), the dependence of the equilibrium potential φ on the hydrogen concentration C_α is[18]

$$\varphi = \varphi_o - \frac{RT}{F} \ln\left(\frac{C_\alpha}{N - C_\alpha}\right) \quad [52]$$

where $\varphi_o = -RT/F \ln(a_{OH}/K_1K_2a_{H_2O}) = -1.06$ V is the equilibrium potential at $C_\alpha/N = 0.5$ (or $X_\alpha = 0.5$).[18] The state of discharge for the single-phase electrode is defined as

$$(SOD)_\alpha = \frac{C_{\alpha max} - C_\alpha}{C_{\alpha max}} = 1 - \frac{C_\alpha}{C_{\alpha max}} \quad [53]$$

If we consider a potential φ = −1.08 V (corresponding to p_{H_2} = 1 atm) as the fully charged state, the bulk concentration for solid solution phase electrode is $C_{\alpha max}$. N is the available concentration of hydrogen, thus X_m can be calculated as[18]

$$X_m = \frac{C_{\alpha max}}{N} = 0.69 \quad [54]$$

by substituting Eq. 53 and 54 into 52, we obtain

$$\varphi = -1.06 - \frac{RT}{F} \ln\left(\frac{1 - (SOD)_\alpha}{0.45 + (SOD)_\alpha}\right) \quad [55]$$

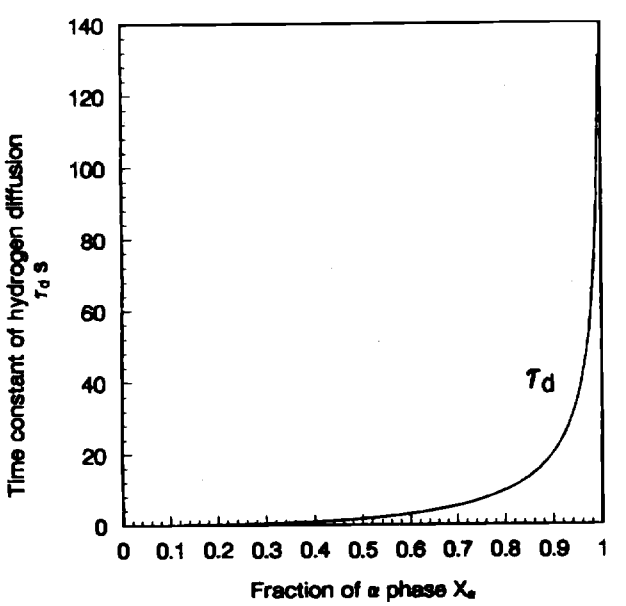

Fig. 4. The time constant of hydrogen diffusion τ_d vs. fraction of α phase X_α. The τ_d is simulated based on Eq. 49 with parameters of $D = 10^{-8}$ cm²/s.

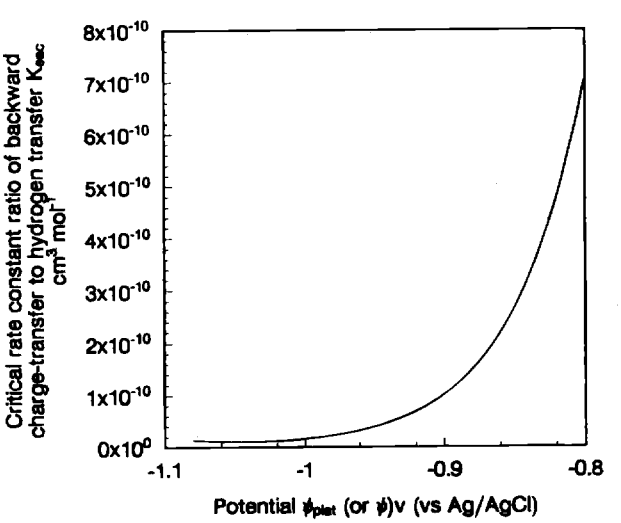

Fig. 5. Relationship between plateau potential φ_{plat} (or potential φ) and K_{eac}, which is calculated from Eq. 50.

by combining Eq. 36, 40-44, 46, and 55, the impedance of the single-phase electrode at different $(SOD)_\alpha$ can be obtained. Figure 8 shows the simulated impedance for the single-phase electrode with the parameters of $k_{-1} = 3.29 \times 10^{-15}$ cm s^{-1}, $k_{-2} = 2.37 \times 10^{-5}$ mol cm^{-2} s^{-1}, $D = 10^{-8}$ cm^2 s^{-1} at 10, 50, 80, 90, and 98% $(SOD)_\alpha$. As $(SOD)_\alpha$ increases from 10 to 98% the potential increases from −1.08 to −0.95 V according to Eq. 55. Because $K_{ea} = 2.77 \times 10^{-10}$ cm^3 mol^{-1} > K_{eac}, and $K_{ad} = 2.37 \times 10^3$ mol cm^4 > K_{adc} in the potential range between −1.08 and −0.95 V (see Fig. 5 and 6 as $X_\alpha = 1$), the arc in the higher frequency range corresponds to the charge-transfer reaction, the curve in the middle frequency corresponds to the hydrogen transfer reaction, and the arc in the low frequency range corresponds to the hydrogen diffusion reaction. As we expected in the above section using the dimensionless parameters K_{ea}/K_{eac} and K_{ad}/K_{adc} at different potential with increasing $(SOD)_a$ (i.e., increasing potential) the two arcs in the high frequency range move toward the low frequency range and the resistance of the three steps increases in the following order

hydrogen diffusion > hydrogen transfer reaction

> charge-transfer reaction

Therefore the two arcs in the high frequency range are gradually being overlapped by the arc of hydrogen diffusion due to fast increasing R_d with increasing $(SOD)_\alpha$. For impedance of hydrogen diffusion, in the higher frequency range, where the penetration of the concentration wave is small compared to the radius of the particle, the impedance shows the Warburg impedance of $\sigma/\sqrt{2\omega D}\ (1 - j)$ series with a capacitance of C_1 (= r_o/σ) (see Appendix and Fig. 9a). At the low frequency range the penetration depth increases beyond the radius of the particle, the impedance corresponds to a resistance of R_1 (= $r_o\sigma/5D$) in series with a capacitance of C_2 (= $r_o/3\sigma$) (see Appendix and Fig. 9b), which reflects the fact that a source with a limited concentration cannot deliver a finite flux.

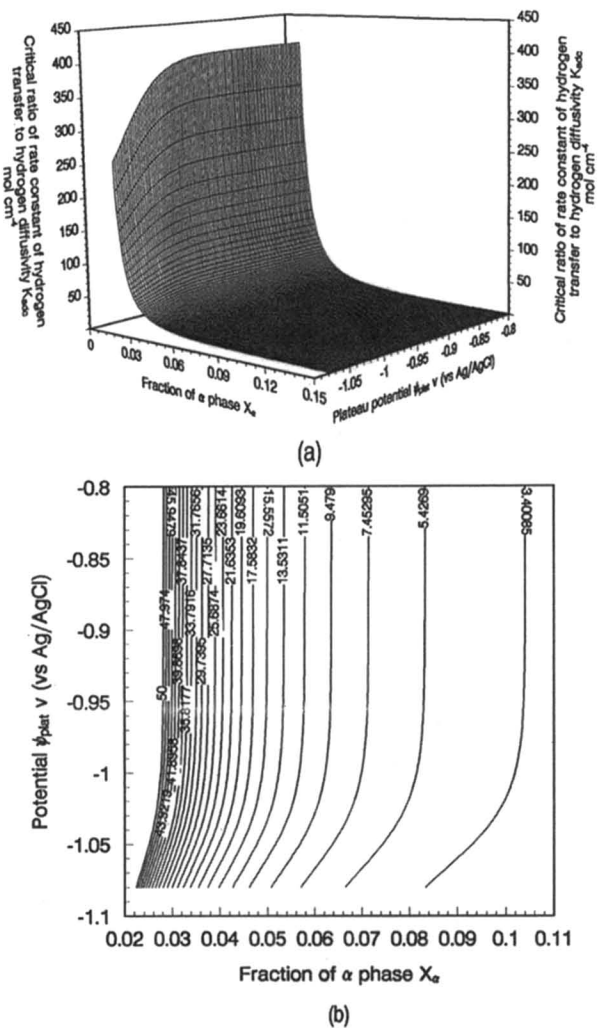

Fig. 6. Relationship between plateau potential φ_{plat} (or potential φ), fraction of α phase X_α, and K_{adc}, which is calculated from Eq. 51. (a) Three-dimensional curved surface and (b) iso-K_{adc} section.

Effect of state of discharge on the EIS of a two-phase electrode with spherical symmetry.—If the plateau pressure of hydrogen is at 1 atm, the discharge capacity for a (α + β) two-phase electrode can be divided into two parts. One is the hydrogen desorption during the β → α phase transformation, the other is the hydrogen desorption from the single α phase. Therefore the state of the discharge for (α + β) two-phase electrode is defined as

$$(SOD)_{\alpha\beta} = \frac{C_\beta - C}{C_\beta} \quad [56]$$

$$(SOD)_{\alpha\beta} = X_\alpha\left(1 - \frac{C_{\alpha\,max}}{C_\beta}\right) \quad \text{when} \quad (\text{SOD})_{\alpha\beta} < 1 - \frac{C_{\alpha\,max}}{C_\beta} \quad [57]$$

$$(SOD)_{\alpha\beta} = 1 - (1 - (SOD)_\alpha)\frac{C_{\alpha\,max}}{C_\beta}$$

$$\text{when} \quad (\text{SOD})_{\alpha\beta} > 1 - \frac{C_{\alpha\,max}}{C_\beta} \quad [58]$$

At the latter discharge state, i.e., $(SOD)_{\alpha\beta} > 1 - C_{\alpha max}/C_\beta$, the relationship between $(SOD)_\alpha$ and the EIS has been discussed in the above section. Here we only analyze the effect of X_α on EIS.

It can be seen from Eq. 40-46 that the fraction of α-phase X_α affects only the arc of the hydrogen diffusion as shown in Fig. 10. In the high frequency range the impedance for finite spherical hydrogen diffusion in the two-phase electrode shows the Warburg impedance of $\sigma/\sqrt{2\omega D}$ $(1 - j)$ in series with a capacitance of C_1 (= r_o/σ) as shown in Fig. 9a (see Appendix), which is the same as the impedance for finite spherical hydrogen diffusion in the single-phase electrode. But in the low frequency range the impedance for finite spherical hydrogen diffusion in the two-phase electrode now corresponds to a resistance of R_2 (= $\sigma r_o[1 - (1 - X_\alpha)^{1/3}]/D(1 - X_\alpha)^{1/3}$) in parallel with $R_3 - C_3$ series with the values of $r_o[1 - (1 - X_\alpha)^{1/3}]\sigma/5D$ and $r_o[1 - (1 - X_\alpha)^{1/3}]/3\sigma$, respectively (see Appendix and Fig. 9c).

In Fig. 10 with increasing x_σ [i.e., increasing $(SOD)_{\alpha\beta}$] the arc of infinite spherical hydrogen diffusion moves gradually toward low frequency range due to the increase of the time constant of hydrogen diffusion (see Fig. 4). At the same time the resistance of hydrogen diffusion increases rapidly, the radius of the almost circular low frequency segment increases toward the limit of a $r_o\sigma/5D$ resistance in series with capacitance of $r_o/3\sigma$ for $X_\alpha = 1$. From Fig. 9 and 10 we conclude that for the spherical hydride electrode with flat pressure plateau, when $(SOD)_{\alpha\beta}$ increases, the almost circular low-frequency segment moves toward low frequency range and its radius increases toward the $R_1 - C_2$ series for $X_\alpha = 1$, (i.e., $R_2 \to \infty$, $R_3 \to R_1$ for $X_\alpha \to 1$). After the β → α phase transformation is complete, the arcs of the charge-transfer reaction and hydrogen transfer reaction move further toward the low frequency range and the resistances of the three steps (i.e., R_{ct}, R_{ab}, and R_d) increase, especially for R_d. Finally the two arcs in the high frequency range are overlapped by the arc of hydrogen diffusion. The EIS of the two-phase electrode at different $(SOD)_{\alpha\beta}$ have confirmed the predicted results using the dimensionless parameters K_{ea}/K_{eac} and K_{ad}/K_{adc}. In practice the pressure plateau of hydrogen for the hydride electrode is slanted, i.e., with β → α phase transformation the electrode potential increases gradually. So, with the increasing state of discharge both X_α and $(SOD)_\alpha$ affect the imped-

ance of the hydride electrode. The effect of $(SOD)_{\alpha\beta}$ on EIS of the two-phase electrode is in agreement with the experimental results of the $M_mNi_{3.5}Co_{0.7}Al_{0.8}$ electrode reported by Kuriyama et al.[11]

Effect of the pressure plateau of hydrogen on EIS of the two-phase electrode with spherical symmetry.—The pressure of hydrogen can be converted to the potential according to the Nernst equation.[18] Here we discuss the effect of plateau potential on EIS. The impedance of the two-phase electrode at different plateau potentials is calculated from Eq. 36, 40-43, 45-46 and substitution of φ_{plat} for φ as shown in Fig. 11. Comparing Fig. 11 with Fig. 8 we can see that φ_{plat} and $(SOD)_\alpha$ have similar effects on the EIS in the high frequency range, since potential φ of the single-phase electrode is related to $(SOD)_\alpha$ (see Eq. 55) and the equivalent circuits of both single- and two-phase electrodes in the high frequency range are the same (see Fig. 9a). But a large EIS difference exists at low frequency since their equivalent circuits at low frequency are quite different. For the single-phase electrode, the equivalent circuit at low frequency is a resistance R_1 in series with a capacitance C_2, but for the two-phase electrode the equivalent circuit in the low frequency range is a resistance of R_2 in parallel with $R_3 - C_3$ series as shown in Fig. 9b and c. Also the arc radius of the hydrogen diffusion increases with increasing plateau potential, but its characteristic frequency remains constant.

Effect of the rate constant of the charge-transfer reaction on EIS of the two-phase electrode with spherical symmetry.—The Nyquist plots of two-phase electrodes with different k_1 are illustrated in Fig. 12. Since K_1 (= k_{-1}/k_1 = 0.94) and K_{eac} are constant at certain electrode potential (see Eq. 50), with increasing k_1, K_{ea}/K_{eac} increases, but R_{ct} decreases (see Eq. 40). Therefore the arc of the charge-transfer reaction moves toward the high frequency range and its radius decreases with k_1 increasing. In Fig. 12 when k_1 is small (1.75×10^{-15} cm s^{-1}), the two arcs in the higher frequency range overlap (Fig. 12, curve a) because the values of K_{ea}/K_{eac} (= 4.27) and R_{ab}/R_{ct} (= 2.27) are around 1 at a potential of −1 V. As k_1 increases to 3.5×10^{-15} m s^{-1} the arc of the charge-transfer reaction separates from the arc of the hydrogen-transfer reaction (Fig. 12, curve b) owing to the larger value of K_{ea}/K_{eac} (= 8.54). If k_1 increases further to 3.5×10^{-13} cm s^{-1}, the arc of the charge-transfer reaction is overlapped again by the arc of the hydrogen-transfer reaction (Fig. 12, curve d) due to the larger R_{ab}/R_{ct} (= 90.9).

Effect of the rate constant of hydrogen transfer between the absorbed state and adsorbed state on EIS of the two-

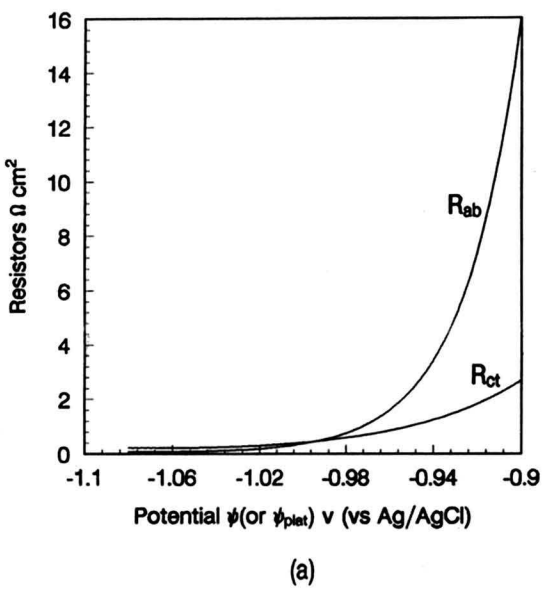

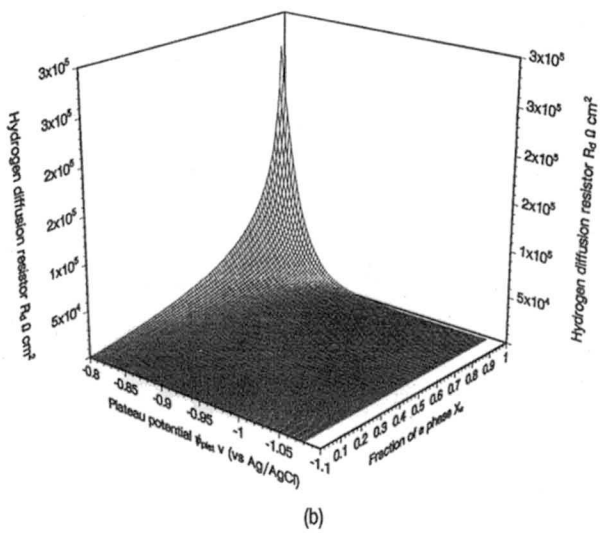

Fig. 7. The resistances of three steps vs. the plateau potential and fraction of α phase X_α: (a) R_{ct} and R_{ab} vs. φ_{plat} (or potential φ) simulated from Eq. 40 and 42 with the parameters of k_{-1} = 3.289×10^{-15} cm s^{-1}, $k_{-2} = 2.37 \times 10^{-5}$ mol cm^{-2} s^{-1}, respectively. (b) Three-dimensional curved surface of R_d vs. φ_{plat} and X_α, (c) iso-R_d section. The R_d is calculated from the following equation with $D = 10^{-8}$ cm^2 s^{-1}.

$$R_d = R_2 + R_3 = \frac{r_o\sigma[1-(1-X_\alpha)^{1/3}]}{D}\left[\frac{1}{(1-X_\alpha)^{1/3}} + \frac{1}{5}\right]$$

$$= \frac{1.33 \times 10^{-8}}{D}\left[1.56 \times 10^{9}\ \exp(19.48\varphi_{plat}) + \frac{1}{1.56 \times 10^{9}\ \exp(19.48\varphi_{plat})}\right]^2 [1-(1-X_\alpha)^{1/3}]\left(\frac{1}{(1-X_\alpha)^{1/3}} + \frac{1}{5}\right)$$

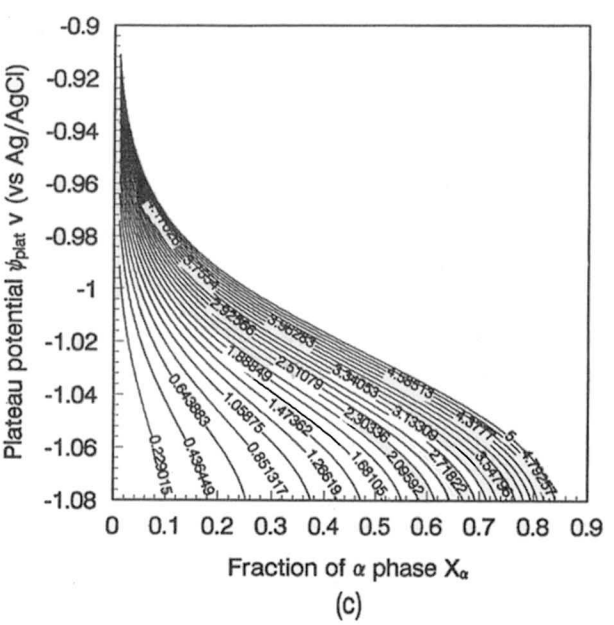

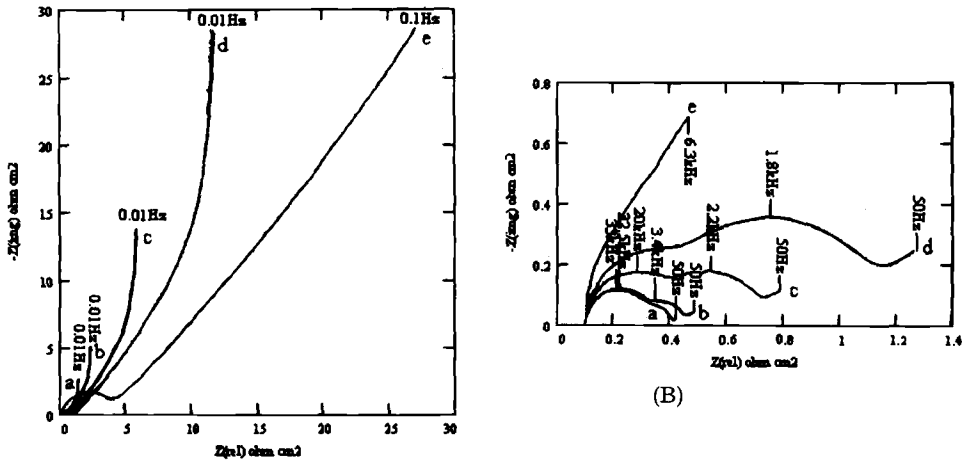

Fig. 8. Nyquist plots for the single-phase electrode with spherical symmetry simulated based upon Eq. 36, 40-44, 46, and 55 at different states of discharge: (a) fully charged state, (b) 50% $(SOD)_\alpha$, (c) 80% $(SOD)_\alpha$, (d) 90% $(SOD)_\alpha$, (e) 98% $(SOD)_\alpha$, with the parameters of k_{-1} = 3.289 × 10^{-15} cm s^{-1}, k_{-2} = 2.37 × 10^{-15} mol cm^{-2} s^{-1}, D = 10^{-8} cm^2 s^{-1}. (B, right) An enlargement of Nyquist plots (A) at the higher frequency range.

phase electrode with spherical symmetry.—The Nyquist plots of two-phase electrodes with different k_2 are illustrated in Fig. 13. Since K_2 (= 2.37), K_{eac} and K_{adc} are constants at a certain electrode potential and state of discharge; with increasing k_2 both K_{ea}/K_{eac} and R_{ab} decrease but K_{ad}/K_{adc} increases. Therefore the arc of the hydrogen-transfer reaction moves toward the high frequency range and its radius decreases with increasing k_2. At k_2 = 10^{-4} mol cm^{-2} s^{-1} the reaction rate for the hydrogen transfer is faster than that for the charge-transfer reaction, but the arc of hydrogen-transfer reaction is overlapped by the charge-transfer reaction due to a small resistance R_{ab} and value of $1 - K_{ea}/K_{eac}$ (= 0.15).

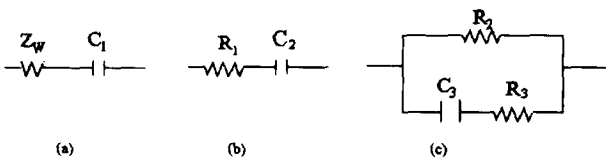

Fig. 9. Equivalent circuit for finite spherical hydrogen diffusion: (a) single- and two-phase electrode in high frequency range, (b) single-phase electrode in low frequency range, (c) two-phase electrode in low frequency range. Where $Z_w = \sigma/\sqrt{2\omega D}\,(1 - j)$, $C_1 = r_o/\sigma$, $C_2 = r_o/3\sigma$, $C_3 = r_o[1 - (1 - X_\alpha)^{1/3}]/3\sigma$, $R_1 = \sigma r_o/5D$, $R_2 = \sigma r_o[1 - (1 - X_\alpha)^{1/3}]/D(1 - X_\alpha)^{1/3}$, $R_3 = r_o[1 - (1 - X_\alpha)^{1/3}]\sigma/5D$. If $X_\alpha \rightarrow 1$, then $C_3 \rightarrow C_2$, $R_2 \rightarrow \infty$, and $R_3 \rightarrow R_1$.

Effect of the diffusion coefficient of hydrogen D on EIS of the two-phase electrode with spherical symmetry.—With increasing diffusion coefficient of hydrogen, the values of K_{ad}/K_{adc} and R_d decrease. Therefore the arc of hydrogen diffusion moves toward higher frequency and its resistance becomes smaller as shown in Fig. 14. When the diffusion coefficient is small, the arc of the hydrogen-transfer reaction is overlapped by the arc of the hydrogen diffusion due to the larger resistance of hydrogen diffusion.

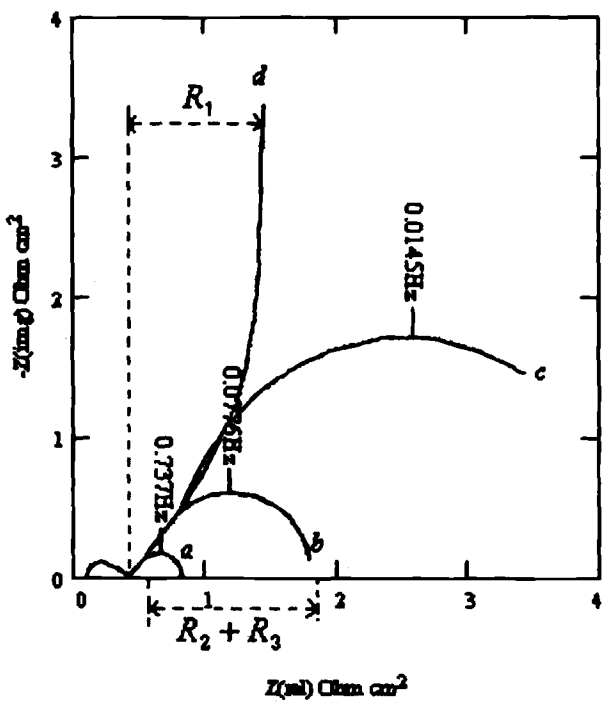

Fig. 10. Nyquist plots for the two-phase electrode with spherical symmetry simulated based upon Eq. 36, 40-43, and 45-46 at different fraction of the α phase X_α: (a) 0.2, (b) 0.5, (c) 0.8, (d) 1, with the parameters of φ_{plat} = 1.08 V vs. Ag/AgCl, k_{-1} = 3.289 × 10^{-15} cm s^{-1}, k_{-2} = 2.37 × 10^{-5} cm^{-2} s^{-1}, D = 10^{-8} cm^2 s^{-1}.

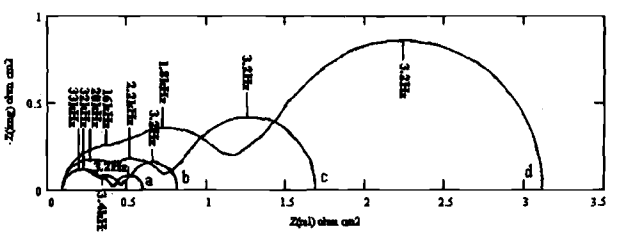

Fig. 11. Nyquist plots for the two-phase electrode with spherical symmetry simulated based upon Eq. 36, 40-43, and 45-46 at different potential plateaus φ_{plat} V vs. Ag/AgCl: (a) −1.08, (b) −1.043, (c) −1.012, (d) −0.992, with the parameter of X_α = 0.1, k_{-1} = 3.289 × 10^{-15} cm s^{-1}, k_{-2} = 2.37 × 10^{-5} mol cm^{-2} s^{-1}, D = 10^{-8} cm^2 s^{-1}.

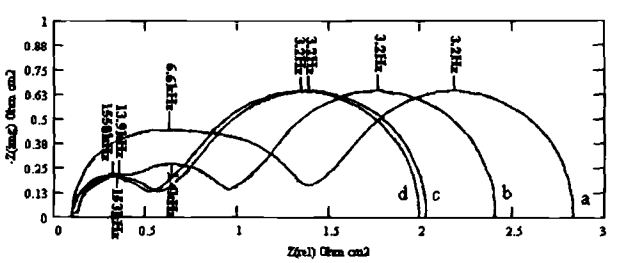

Fig. 12. Nyquist plots for the two-phase electrode with spherical symmetry simulated based upon Eq. 36, 40-43, and 45-46 at different rate constant of charge-transfer reaction k_1 cm s^{-1}: (a) 1.751 × 10^{-15}, (b) 3.502 × 10^{-15}, (c) 3.502 × 10^{-14}, (d) 3.502 × 10^{-13}, with the parameters of X_α = 0.1, φ_{plat} = −1 V vs. Ag/AgCl, k_{-2} = 2.37 × 10^{-5} mol cm^{-2} s^{-1}, D = 10^{-8} cm^2 s^{-1}.

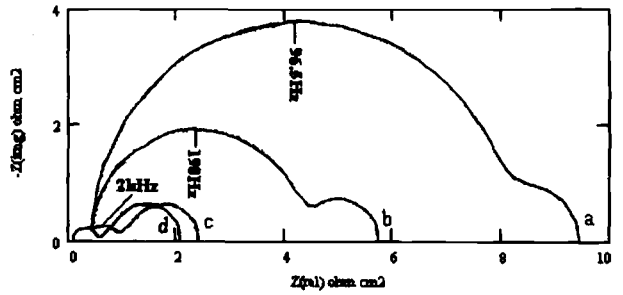

Fig. 13. Nyquist plots for the two-phase electrode with spherical symmetry simulated based upon Eq. 36, 40-43, and 45-46 at different rate constant of hydrogen transfer reaction k_2 mol cm^{-2} s^{-1}: (a) 5×10^{-7}, (b) 10^{-6}, (c) 10^{-5}, (d) 10^{-4}, with the parameters of $X_\alpha = 0.1$, $\varphi_{plat} = -1$ V vs. Ag/AgCl, $k_{-1} = 3.289 \times 10^{-15}$ cm s^{-1}, $D = 10^{-8}$ cm^2 s^{-1}.

Effect of other factors on EIS of the two-phase electrode with spherical symmetry.—Zhang et al. have studied the impedance of the La-Ni-Co-Mn-Al electrode with different area of current collector and different kind of binder materials.[9] Their Nyquist plots can be explained well by the present simulation results.

1. Effect of amount of alloy on EIS: in the present Nyquist plots the unit of resistance and capacitance is in Ω cm^2 and F cm^{-2}, respectively. Increasing the amount of alloy will provide a more active area. Therefore it decreases the resistances of three steps (in Ω units) but increases the capacitances of three steps (in F units), especially for the resistance of hydrogen diffusion due to its larger resistance and capacitance. However it does not affect the time constant (or its characteristic frequency), since the time constant ($R \times C$) is independent of active areas. Figure 14 in Ref. 9 also confirmed that the time constant ($R \times C$) for the arc in the low frequency range remains constant with increasing amount of alloy.

2. Effect of the contact area between the current collector and the alloy on EIS: increasing the contact area between the current collector and the alloy will increase the total active area and double-layer capacitance, the electrode with large contact area between the current collector and pellet has small R_{ct} (unit in Ω) but large C_{dl} (unit in F). Therefore the time constant τ_c (= $R_{ct} \times C_{dl}$) remains constant. Figure 10 in Ref. 9 also shows that the contact area only decreases the radius of arc in the high frequency range but does not affect the reaction rate in higher frequency range.

3. Effect of the binder materials on EIS: the electrodes made with different binders have a different area between the absorption and adsorption, which results in a change of R_{ab} (unit in Ω) and C_{ad} (unit in F) in reversal direction. Since the time constant τ_a is independent of area between the absorption and adsorption, the characteristic frequency remains stable. By examining Fig. 11 in Ref. 9, we also find that the kind of binder materials used only affects the radius of the arc in middle frequency range but has no influence on its frequency range.

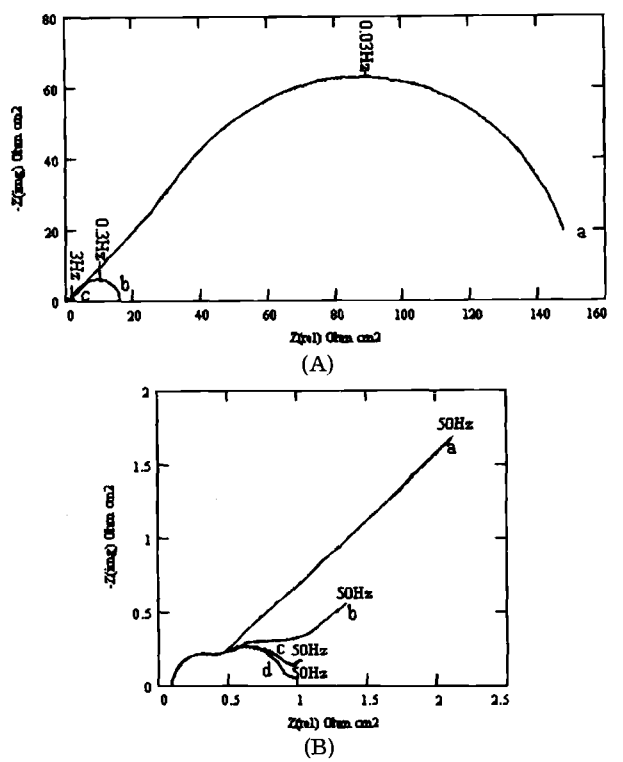

Fig. 14. Nyquist plots for the two-phase electrode with spherical symmetry simulated based upon Eq. 36, 40-43, and 45-46 at different diffusion coefficient D cm^2 s^{-1}: (a) 10^{-10}, (b) 10^{-9}, (c) 10^{-8}, (d) 10^{-7}, with the parameters of $X_\alpha = 0.1$, $\varphi_{plat} = -1$ V vs. Ag/AgCl, $k_{-1} = 3.289 \times 10^{-15}$ cm s^{-1}, $k_{-2} = 2.37 \times 10^{-5}$ mol cm^{-2} s^{-1}. (B) An enlargement of the Nyquist plots (A) at the higher frequency.

Conclusions

A mathematical model for the electrochemical impedance spectroscopy of a metal-hydride electrode was developed. The model was used to study the effect of various parameters on predicted kinetic behavior and the experimental results reported by Zhang et al.[9] can be explained by the present model satisfactorily.

The simulations obtained using the model show that the first arc appearing in the higher frequency range is due to the charge-transfer reaction, the second arc in the middle frequency range represents the hydrogen transfer between the absorption and adsorption, and the third arc (or curve) at low frequency corresponds to the diffusion of absorbed hydrogen through the alloy. As the rate constant of the charge-transfer reaction, the rate constant of hydrogen transfer and the diffusion coefficient of hydrogen increase, the three arcs (or curve of hydrogen diffusion for single-phase electrode) move toward higher frequency range and the radius of the three arcs decrease.

For two-phase electrode with flat pressure plateau, at the high frequency range the impedance for finite spherical hydrogen diffusion shows the Warburg impedance of $\sigma/r_o\sqrt{2\omega D}$ in series with a capacitance of r_o/σ, but in the low frequency range it corresponds to a resistance of $\sigma r_o[1 - (1 - X_\alpha)^{1/3}]/D(1 - X_\alpha)^{1/3}$ in parallel with a resistance-capacitance series which have the value of $r_o[1 - (1 - X_\alpha)^{1/3}]/3\sigma$ and $r_o[1 - (1 - X_\alpha)^{1/3}]\sigma/5D$, respectively. When the state of discharge increases, the arc in the low frequency range moves toward the lower frequency range and the radius of the almost circular low-frequency segment increases toward a resistance of $r_o\sigma/5D$ in series with a capacitance of $r_o/3\sigma$ for $X_\alpha = 1$. After the $\beta \rightarrow \alpha$ phase transformation is complete the arcs of charge-transfer reaction and hydrogen transfer move further toward the low frequency range and the resistances of the three steps increase. Finally the arcs overlap. In practice the pressure plateau of hydrogen for hydride electrode is slanted, i.e., during the $\beta \rightarrow \alpha$ phase transformation the electrode potential is not stable, but increases gradually. So with the increasing state of discharge the mixing effect of X_α and $(SOD)_\alpha$ affects the impedance of hydride electrode.

Acknowledgments

The author acknowledges the financial support from the National Natural Science Foundation of China (no. 59502005). The author is also grateful to Dr. H. Bakker, Van der Waals-Zeeman Laboratory, University of Amsterdam, and Dr. X. H. Wang, Department of Materials Science and Engineering, Zhejiang University, for revising this paper.

Manuscript submitted April 18, 1997; revised manuscript received December 22, 1997.

Zhejiang University assisted in meeting the publication costs of this article.

APPENDIX

Impedance of finite hydrogen diffusion in the two-phase electrode with spherical symmetry.—The solution for finite spherical diffusion is obtained from Eq. 36 and 39

$$Z_d = \frac{\sigma}{\sqrt{j\omega D}\coth\left[r_o(1-(1-X_\alpha)^{1/3})\sqrt{\frac{j\omega}{D}}\right] - \frac{D}{r_o}} \quad [A\text{-}1]$$

High-frequency limit.—The behavior at high frequency is obtained from Eq. A-1 and the limit

$$\omega \to \infty,\ \coth\left[r_o(1-(1-X_\alpha)^{1/3})\sqrt{\frac{j\omega}{D}}\right] \to 1$$

$$Z_d = \frac{\sigma}{\sqrt{j\omega D} - \frac{D}{r_o}} = \frac{r_o\sigma}{D\left(r_o\sqrt{\frac{j\omega}{D}} - 1\right)}$$

$$\approx \frac{r_o\sigma}{Dr_o\sqrt{\frac{j\omega}{D}}}\left(1 + \frac{1}{r_o\sqrt{\frac{j\omega}{D}}}\right) = \frac{\sigma}{\sqrt{2\omega D}}(1-j) + \frac{\sigma}{j\omega r_o}$$

$$= Z_w + \frac{1}{j\omega C_1} \quad [A\text{-}2]$$

equivalent to a Warburg impedance in series with a capacitance of C_1.

Low-frequency limit.—Introducing the first three terms of the low-frequency approximation

$$\omega \to 0 \to \coth\left[r_o(1-(1-X_\alpha)^{1/3})\sqrt{\frac{j\omega}{D}}\right]$$

$$\approx \frac{1}{r_o(1-(1-X_\alpha)^{1/3})\sqrt{\frac{j\omega}{D}}} + \frac{r_o(1-(1-X_\alpha)^{1/3})\sqrt{\frac{j\omega}{D}}}{3}$$

$$- \frac{\left\{r_o(1-(1-X_\alpha)^{1/3})\sqrt{\frac{j\omega}{D}}\right\}^3}{45} \quad [A\text{-}3]$$

The admittance of finite hydrogen diffusion

$$Y_d = \frac{\sqrt{j\omega D}}{\sigma}\coth\left[r_o(1-(1-X_\alpha)^{1/3})\sqrt{\frac{j\omega}{D}}\right] - \frac{D}{r_o\sigma} \quad [A\text{-}4]$$

Substitute Eq. A-3 into Eq. A-4

$$Y_d = \frac{D(1-X_\alpha)^{1/3}}{\sigma r_o[1-(1-X_\alpha)^{1/3}]} + \frac{r_o[1-(1-X_\alpha)^{1/3}]j\omega}{3\sigma}\left[1 - \frac{\{r_o[1-(1-X_\alpha)^{1/3}]\}^2 j\omega}{15D}\right]$$

$$\approx \frac{D(1-X_\alpha)^{1/3}}{\sigma r_o[1-(1-X_\alpha)^{1/3}]} + \frac{r_o[1-(1-X_\alpha)^{1/3}]j\omega}{3\sigma} \times \frac{1}{1 + \frac{\{r_o[1-(1-X_\alpha)^{1/3}]\}^2 j\omega}{15D}} = \frac{D(1-X_\alpha)^{1/3}}{\sigma r_o[1-(1-X_\alpha)^{1/3}]} + \frac{1}{\frac{3\sigma}{r_o[1-(1-X_\alpha)^{1/3}]j\omega} + \frac{\sigma r_o[1-(1-X_\alpha)^{1/3}]}{5D}} \quad [A\text{-}5]$$

The impedance of the finite hydrogen diffusion

$$Z_d = \frac{1}{\frac{1}{R_2} + \frac{1}{\frac{1}{j\omega C_3} + R_3}} \quad [A\text{-}6]$$

where

$$R_2 = \frac{\sigma r_o[1-(1-X_\alpha)^{1/3}]}{D(1-X_\alpha)^{1/3}},\quad R_3 = \frac{\sigma r_o[1-(1-X_\alpha)^{1/3}]}{5D},$$

$$C_3 = \frac{r_o[1-(1-X_\alpha)^{1/3}]}{3\sigma}$$

equivalent to a resistance of R_2 parallel with $R_3 - C_3$ series. When $X_\alpha \to 1$, the $R_2 \to \infty$, $C_3 \to r_o/3\sigma = C_2$

$$R_3 \to \frac{\sigma r_o}{5D} = R_1$$

equivalent to a resistance of R_1 in series with a capacitance of C_2

LIST OF SYMBOLS

α_{OH}, α_{H_2O}	activity of OH^- and H_2O in solution, respectively
$C^o_{H_2O}$, $C^o_{OH^-}$	concentration of H_2O and OH^- in the reference state, respectively, $C^o_{H_2O} = C^o_{OH^-} = 1$ mol/cm^3
C_α, C_β, C_s	concentration of hydrogen in α, β phase and in the near-surface, respectively, in mol/cm^3
C_{ad}, C_{dll}	absorption capacitance and double-layer capacitance, F/cm^2
C_1, C_2, C_3	capacitances in equivalent circuit of finite spherical electrode, F/cm^2
D	diffusion coefficient of hydrogen in the metal particles, cm^2/s
F	Faraday's constant, 96,487 C/mol
f_e^*, f_a^*, f_d^*	characteristic frequency of charge-transfer, hydrogen transfer, and hydrogen diffusion, Hz
i, i_o	current density and exchange current density, respectively, A/cm^2
j	$\sqrt{-1}$
J_{sur}	hydrogen flux on the electrode surface, mol/cm^2
k_1, k_{-1}	forward and backward rate constants of charge-transfer reaction, cm/s
k_2, k_{-2}	rate constant of hydrogen transfer between adsorption and adsorption, mol/cm^2 s
K_1 (= k_{-1}/k_1), K_2 (= k_{-2}/k_2)	equilibrium constant of charge-transfer reaction and hydrogen transfer process, respectively
K_{ea} (= k_{-1}/k_{-2}), K_{ad} (= k_{-2}/D)	ratio of backward rate constant constant of charge-transfer reaction to that of hydrogen transfer reaction (cm^3/mol) and ratio of backward rate constant of hydrogen transfer reaction to diffusion coefficient (mol cm^4), respectively
K_{eac}, K_{adc}	critical ratio of backward rate constant of charge-transfer reaction to that of the hydrogen transfer reaction (cm^3/mol) and critical ratio of backward rate constant of hydrogen transfer reaction to diffusion coefficient (mol cm^4), respectively
N	available concentration of absorbed hydrogen, mol/cm^3
R_s, R_{ct}, R_{ab}	solution resistance, charge-transfer reaction resistance and absorption resistance, respectively; Ω cm^2
R_1, R_2, R_3	resistances in equivalent circuit of finite spherical electrode, Ω cm^2
r_o, r_h	radius of metal particles and radius of untransformed hydride-core phase, cm
SOD	state of discharge of the solid-solution electrode
$(SOD)_{\alpha\beta}$	state of discharge of the two-phase electrode
V_α, V_β	volume of α and β phase, respectively
x_α, x_s	molar concentration quotient of absorbed hydrogen in α phase and molar concentration quotient of hydrogen in subsurface
X_α	fraction of α phase
X_m	solubility of H in the $TiMn_{1.5}$ bulk at 1 atm
Greek	
α, β	symmetry factor in the reduction and oxidation direction, respectively
θ, Γ	coverage degree of adsorbed hydrogen and maximum coverage degree of adsorbed hydrogen,

	mol/cm^2
φ, φ_{plat}	potential of single-phase electrode and plateau potential of two-phase electrode, V vs. Ag/AgCl
φ_o	equilibrium potential at $x_\alpha = 0.5$ V vs. Ag/AgCl
ω	angular frequency of ac single
σ	impedance coefficient of hydrogen diffusion
τ_e, τ_a, τ_d	time constant of charge-transfer, hydrogen transfer and hydrogen diffusion respectively, s

Superscripts

$\rightarrow$, $\leftarrow$	reduction and oxidation direction, respectively
$-$, $\sim$	dc and ac signal

REFERENCES

1. T. Sakai, H. Miyamura, N. Kuriyama, A. Kato, K. Oguro, and H. Ishikawa, *J. Electrochem. Soc.*, **137**, 795 (1990).
2. B. E. Conway and L. Bai, *J. Chem. Faraday Trans.*, **81**, 184 (1985).
3. T. Maoka and M. Enyo, *Electrochim. Acta*, **26**, 607 (1981).
4. G. W. Castellan, *J. Electrochem. Soc.*, **108**, 277 (1961).
5. B. E. Conway and Wojtowicz, *J. Electroanal. Chem.*, **326**, 277 (1992).
6. B. E. Conway and G. Jerkiewicz, *J. Electrochem. Soc.*, **357**, 47 (1993).
7. Q. M. Yang, M. Ciureanu, D. H. Ryan, and J. O. Ström-Olsen, *J. Electrochem. Soc.*, **141**, 2108 (1994).
8. Y. Q. Lei, C. S. Wang, H. G. Pan, J. Wu, and Q. D. Wang, *J. Alloys Compd.*, **231**, 611 (1995).
9. W. Zhang, M. P. S. Kunar, S. Srinivasan, and H. J. Ploehn, *J. Electrochem. Soc.*, **142**, 2935 (1995).
10. C. Lim and S. I. Pyun, *Electrochim. Acta*, **38**, 2645 (1993).
11. N. Kuriyama, T. Sakai, H. Miyamura, I. Vehara, H. Ishikawa, and T. Iwasaki, *J. Electrochem. Soc.*, **139**, 172 (1992).
12. N. Kuriyama, T. Sakai, H. Miyamura, I. Vehara, H. Ishikawa, and T. Iwasaki, *J. Alloys Compd.*, **192**, 161 (1993).
13. C. Wagner, *Z. Phys. Chem.*, **193**, 407 (1994).
14. P. D. Vidts, J. Delgado, and R. E. White, *J. Electrochem. Soc.*, **142**, 4006 (1995).
15. C. Lim and S. I. Pyun, *Electrochim. Acta*, **39**, 363 (1994).
16. D. A. Harrington and B. E. Conway, *Electrochim. Acta*, **32**, 1703 (1987).
17. T. Jacobsen and K. West, *Electrochim. Acta*, **40**, 255 (1995).
18. Q. M. Yang, M. Ciureanu, D. H. Ryan, and J. O. Ström-Olsen, *Electrochim. Acta*, **40**, 1921 (1995).
19. J. Balej, *Int. J. Hydrogen Energy*, **10**, 365 (1985).
20. A. Lasia and D. Gregoire, *J. Electrochem. Soc.*, **142**, 3393 (1995).
21. G. Zhang, B. N. Popov, and R. E. White, *J. Electrochem. Soc.*, **142**, 2695 (1995).

Deposition of Silica Films Using Electrochemical Procedures

Edward A. Speers[a] and J. R. Cahoon

Department of Mechanical and Industrial Engineering, University of Manitoba, Winnipeg, Manitoba, Canada

ABSTRACT

A process whereby a thin surface layer of SiO_2 can be electrochemically deposited on a metallic substrate is described. The process has been termed *silicadizing* and utilizes K_2SiO_3 electrolyte at pH 11-13 with additions of K_2O, Na_2O_2, and CH_3COOH. The metal to be coated is the anode, and direct current voltages up to 350 V at low currents are used. Preliminary tests indicate that various types of silicadized coatings can be produced depending upon possible applications. The coatings can be used as a preparatory adhesive surface for painting of aluminum alloys or as a decorative surface by itself. Initial tests indicate that the silicadized surface layer is both wear resistant and corrosion resistant.

Introduction

Silicadizing is a process that can potentially be used to protect the surface of aluminum and other metals from corrosion and abrasion. Patents were obtained for silicadizing as far back as 1911,[1-5] but the process has never been commercialized successfully, nor has it been featured in the technical literature. The patents report excellent corrosion resistance and wear resistance properties for silicadized aluminum but little is known concerning the nature of the surface coating. The reported properties of the silicadized surface and the process itself appear commercially attractive and, therefore, this present research has been conducted with the objectives of investigating the optimizing the variables of the silicadizing process and of determining the nature of the silicadized surface layer.

The Process

In silicadizing, the aluminum article to be coated is made the anode as in anodizing, but potentials of a few hundred volts are utilized instead of the lower voltages normally used in anodizing. Also, silicadizing uses alkaline electrolytes which are environmentally more acceptable than the acidic solutions used in anodizing. The preferred alkaline electrolytes consist of aqueous solutions of potassium silicates. Potassium silicate solutions are not a controlled product under the Workplace Hazardous Materials Information Systems (WHMIS). It is a nonflammable, stable, aqueous liquid. However, upon long contact with some metals, such as aluminum, tin, lead, or zinc, flammable hydrogen gas may be produced. The amphoteric nature of aluminum and zinc allows the metals to dissolve in an alkaline solution with the evolution of hydrogen and the formation of metal ions. Therefore, only steel drums or other nonreactive containers must be employed. The solution gels upon mixing with acid. In use, normal precautions are necessary as when using any alkali solutions.

The apparatus for silicadizing is shown schematically in Fig. 1. A rectifier with a variable voltage control supplies direct voltage (dc) current to the electrode. Austenitic stainless steel is a suitable material for the cathode since it does not contaminate the electrolyte but nickel and iron can also be used. The anode is the aluminum article to be silicadized (3003-H14 or 2024-T6 alloy) and the electrolyte is an alkaline K_2SiO_3 solution, the composition of which is dependent upon the desired properties of the coating. The electrolytes were prepared from 8.2 M. K_2SiO_3 stock solution with a density of 30° Baumé [b] (sp gr 1.26) by dilution with appropriate amounts of distilled water. Additions of K_2O, Na_2O_2, and CH_3COOH were sometimes made to impart specific properties to the coatings. The aluminum

[a] Present address: Edward A. Speers and Associates, Winnipeg, Manitoba, Canada.

[b] The Baumé scale is the industry standard used for measuring the density of silicate solutions and is therefore used here. The relationship between the Baumé scale and specify gravity (for liquids heavier than H_2O) is given by [6] 2 Bé = 145 − 145/specific gravity where the measurements are conducted at 15.5°C.